

Structural Analysis of the α N-Terminal Region of Erythroid and Nonerythroid Spectrins by Small-angle X-ray Scattering

S. Mehboob,¹ J. Jacob,^{2,3} M. May,¹ L. Kotula,⁴ P. Thiyagarajan,² M.E. Johnson,¹ L.W.-M. Fung⁵

¹Center for Pharmaceutical Biotechnology, University of Illinois at Chicago, Chicago, IL, U.S.A.

²Argonne National Laboratory, Argonne, IL, U.S.A.

³Department of Biochemistry and Molecular Biology, The University of Chicago, Chicago, IL, U.S.A.

⁴Laboratory of Molecular Neurobiology, New York State Institute for Basic Research
in Developmental Disabilities, Staten Island, NY, U.S.A.

⁵Department of Chemistry, Loyola University Chicago, Chicago, IL, U.S.A.

Introduction

Spectrin is a cytoskeletal protein known to control membrane organization, stability, and shape. After spectrin was first identified in erythrocytes, several spectrin isoforms were discovered. These spectrin isoforms probably have key conformational differences in specific regions to provide different functions, and it is crucial to determine these differences in order to understand the functional variations. We used the Sp α I-1-156 peptide (a well-characterized model peptide of the α N-terminal region of erythrocyte spectrin [1]) and Sp α II-1-149 (a Sp α II model peptide similar to Sp α I-1-156 in sequence) to study their conformations in solution by small-angle x-ray scattering (SAXS) methods.

Methods and Materials

The peptides (~2 mg/mL or ~120 μ M) were in 20 mM Tris buffer with 150 mM sodium chloride at pH 7.4. Measurements were carried out at room temperature by using the SAXS instrument at Argonne's APS. Data were collected by using a 15 \times 15-cm, high-resolution, position-sensitive, nine-element tiled, charge-coupled device (CCD) mosaic detector at the BESSRC beamline at the APS [2] or a 4.9 \times 8.6-cm CCD area detector at the Bio-CAT beamline at the APS. The sample-to-detector distance was 2.2 m. At the BESSRC beamline (ID-12), 10 successive 1-second exposures were recorded for each sample (in a thermostated quartz capillary flow cell of 1.5-mm diameter) at room temperature. At the Bio-CAT beamline (ID-18), five successive 10-second exposures were recorded for each sample. Samples were measured under constant-gas-flow conditions to reduce potential radiation damage. No evidence of sample changes was seen over the time interval of exposure.

The measurement of each sample was preceded and followed by a measurement of the same buffer solution used in protein sample preparation. These buffer measurements provided a check on beam properties and the cleanliness of the sample cell between sample measurements as well as the means for background subtraction. For the purpose of obtaining data at high

angles to generate low-resolution shapes of the peptides by using the program GASBOR (see below), the sample-to-detector distance was reduced from 2.2 to 0.8 m. The precision in our experimental procedures, with low protein sample concentrations and small error bars, allowed us to produce data for modeling with GASBOR.

Generally, scattering intensities (I) as a function of Q , where Q is the scattering vector, for Sp α I-1-156 and Sp α II-1-149 were analyzed with established methods [3-5]. The scattering data were subjected to indirect Fourier transformation by using the program GNOM [6] to compute the pair-distance distribution function $P(R)$. R_g values were also calculated from the second moment of the $P(R)$ functions [3, 7]. SAXS data also carry molecular weight information, and such information provides an indication of the sample's aggregation state, which may affect data interpretation. In order to calculate the molecular weight from the SAXS data, the scattering intensity was measured on an absolute scale. A convenient method for obtaining intensity data on an absolute scale is by measuring the scattering intensity of a standard, such as water [8]. We obtained SAXS data for water, by using exactly the same configuration, energy, and geometry as those for the samples, with $d\Sigma/d\Omega = 1.63 \times 10^{-2} \text{ cm}^{-1}$ at 293K, and we obtained a scale factor by comparing the measured angle-independent data and the expected scattering cross section. The scattering intensity data of the samples were then multiplied by the scale factor to place them on an absolute scale.

Results

The measured SAXS profiles (Fig. 1A) showed clear differences between Sp α I-1-156 and Sp α II-1-149 peptides. Since the SAXS profile is sensitive to the size, shape, and internal density distribution of a scattering molecule [9], the differences in the profiles can be attributed to differences in conformations between the two peptides.

The Kratky plots for Sp α I-1-156 and Sp α II-1-149 clearly suggest that Sp α II-1-149 has a relatively more extended structure than Sp α I-1-156. In addition, the $I(Q) \cdot Q^2$ values of both Sp α I-1-156 and Sp α II-1-149

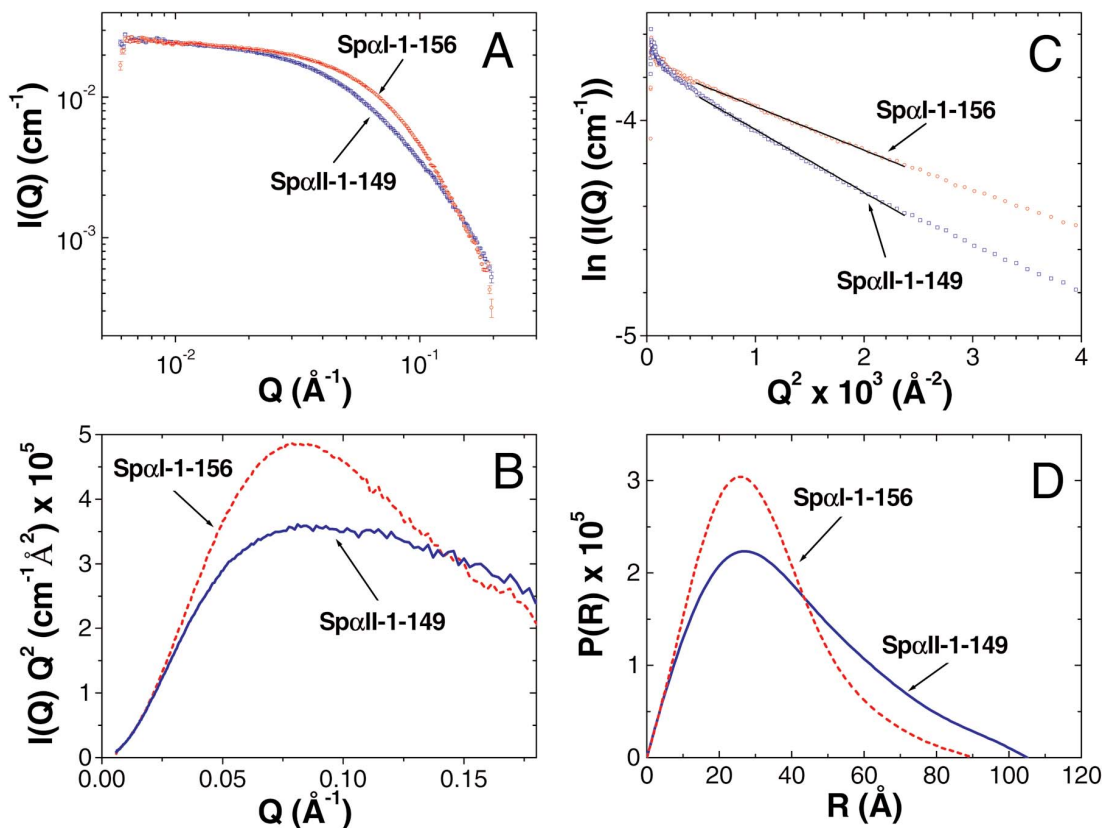


FIG. 1. SAXS data for the two peptides SpαI-1-156 and SpαII-1-149 at room temperature. (A) The solid line represents the best fit to the experimental data for extracting the $P(R)$ functions in part D; representative statistical errors are shown on the experimental data points. (B) Kratky plots of the SAXS data in part A, with the shift in peak position in SpαII-1-149 relative to that of SpαI-1-156 suggesting that SpαII-1-149 has a relatively more expanded structure than SpαI-1-156. (C) Guinier plots of the SAXS data for the SpαI-1-156 and SpαII-1-149 peptides. Data points in the linear Guinier region ($4 \times 10^{-4} \text{ \AA}^{-2} < Q^2 < 2.4 \times 10^{-3} \text{ \AA}^{-2}$ with a solid line fitted to these points as shown) were used to calculate the R_g values (from the slope of the plots in the region where $Q \cdot R_g \leq 1.3$). (D) The distance distribution function $P(R)$ was calculated from the experimental scattering data in part A. The $P(R)$ function was derived by using the program GNOM (30) to fit the entire scattering data.

converge toward zero at low Q , indicating that samples were monomeric and not aggregated. The Guinier plots of the SAXS data for both SpαI-1-156 and SpαII-1-149 (Fig. 1C) exhibit a linear region in the low Q region. The radius of gyration (R_g), obtained from the low Q region ($0.02 \text{ \AA}^{-1} < Q < 0.05 \text{ \AA}^{-1}$) of the Guinier plots (Fig. 1B), is 24.5 \AA for SpαI-1-156 and 29.4 \AA for SpαII-1-149. These values provide a quantitative comparison of the spatial extension of these two peptides. SpαI-1-156, a peptide with seven more amino acid residues, has an R_g value about 20% smaller than that of SpαII-1-149. In addition, the molecular weight analysis from the I_0 values at the y-intercept of the fits in the Guinier plots showed that the molecular weights for SpαI-1-156 and SpαII-1-149 were within 10% of the expected molecular masses of the peptides in

monomeric form, further indicating the absence of any aggregation in the solutions of the samples. Our $P(R)$ profiles obtained from the fits to the SAXS data from using the indirect Fourier transform method for both SpαI-1-156 and SpαII-1-149 are asymmetric (Fig. 1D), indicating asymmetrically shaped peptides. The curve for SpαII-1-149 is more asymmetric than that for SpαI-1-156. Both $P(R)$ profiles peak around 20 \AA . We suggest that these distances correspond to the short intramolecular distances, mainly within the triple helical bundle structural domain (observed for both peptides). The lone helix (Helix C') in SpαI-1-156 exhibits multiple orientations with respect to the triple helical bundle. Hence, the distances between the Helix C' and the triple helical bundle would vary and thus become effectively lower than the probable distances

within the triple helical bundle, such that this distance distribution is masked by the distance distribution profile for the triple helical bundles.

Discussion

The molecular shape studies by SAXS methods clearly indicate a more extended conformation for Sp α II-1-149 than for Sp α I-1-156. All the R_g values obtained by two different analyses of SAXS data and by modeling show a value of about 25 Å for Sp α I-1-156 and about 30 Å for Sp α II-1-149, despite the fact that Sp α I-1-156 has seven amino acid residues than does Sp α II-1-149. We suggest that Sp α I-1-156 exhibits a more flexible conformation than Sp α II-1-149 at the junction region linking Helix C' to the first structural domain.

It is often assumed that spectrin flexibility is the molecular origin of the unique deformability and elasticity of erythrocytes [10]. These studies suggest that erythrocyte spectrin exhibits segmental motions with a highly flexible region connecting more rigid structural elements. In contrast, it has been suggested that brain spectrin is more rigid than erythrocyte spectrin [11]. The SAXS findings for Sp α I-1-156 support our nuclear magnetic resonance (NMR) results [12, 13], consistent with a *flexible junction* between Helix C' and the triple helical bundle that allows multiple orientations between these two structural elements. The SAXS findings for Sp α II-1-149 support the hypothesis that this junction region is rigid (and probably helical) for Sp α II brain spectrin. We also note that our SAXS experiment on Sp α II-1-149 is the first structural study for the brain spectrin N-terminal region.

Acknowledgments

Use of the APS was supported by the U.S. Department of Energy, Office of Science, Office of Basic Energy Sciences, under Contract No. W-31-109-

ENG-38. In addition, Bio-CAT was also funded by the National Institutes of Health (NIH), and NIH National Center for Research Resources (NCR). We acknowledge the invaluable assistance of E. Kondrashkina at Bio-CAT and S. Seifert at BESSRC on SAXS experiments. This work was supported by grants from the National Science Foundation and American Heart Association Midwest Affiliate (to L.W.-M. Fung), the NIH (to L. Kotula, M.E. Johnson, and L.W.-M. Fung), and the Packard Foundation Interdisciplinary Science Program (99-8327) (to P. Thiyagarajan).

References

- [1] S. Mehboob, B.-H. Luo, B.M. Patel, and L.W.-M. Fung, *Biochemistry* **40**, 12457-12464 (2001).
- [2] S. Seifert, R.E. Winans, D.M. Tiede, and P.J. Thiyagarajan, *Appl. Crystallogr.* **33**, 782-784 (2000).
- [3] X. Fang, K. Littrell, X.-J. Yang, S.J. Henderson, S. Seifert, P. Thiyagarajan, T. Pan, and T.R. Sosnick, *Biochemistry* **39**, 11107-11113 (2000).
- [4] V. Receveur, M. Czjzek, M. Schulein, P. Panine, and B. Henrissat, *J. Biol. Chem.* **277**, 40887-40892 (2002).
- [5] A. Guinier and G. Fournet, *Small Angle Scattering of X-rays* (John Wiley and Sons, New York, NY, 1955).
- [6] D.I. Svergun, *J. Appl. Crystallogr.* **25**, 495-503 (1992).
- [7] D. Heidorn and J. Trehwella, *Biochemistry* **27**, 909-915 (1988).
- [8] D. Orthaber, A. Bergmann, and O. Glatter, *J. Appl. Crystallogr.* **33**, 218-225 (2000).
- [9] O. Glatter and O. Kratky, editors, *Small Angle X-ray Scattering* (Academic Press, London, England, 1982).
- [10] B.G. Vertessy and T.L. Steck, *Biophys. J.* **55**, 255-262 (1989).
- [11] G.E. Begg, M.B. Morris, and G.B. Ralston, *Biochemistry* **36**, 6977-6985 (1997).
- [12] S. Park, M. Caffrey, M.E. Johnson, and L.W.-M. Fung, *J. Biol. Chem.* **278**, 21837-21844 (2003).
- [13] S. Park, M.E. Johnson, and L.W.-M. Fung, *FEBS Lett.* **485**, 81-86 (2000).